Research Article

Open Access Journal of
Biomedical Science
ISSN: 2690-487X

Diffusion Weighted Magnetic Resonance Imaging Revealed Changes in the Somatosensory and Motor Cortex of a Mild Relapsing-Remitting Experimental Autoimmune Encephalitis Mouse Model

Othman I Alomair[1,2], Nematullah Khan[3,4], Maree T Smith[3,4], Ian M Brereton[1], Graham J Galloway[1] and Nyoman D Kurniawan[1]*

[1]*Centre for Advanced Imaging, The University of Queensland, Australia*

[2]*College of applied medical science, King Saud University, Saudi Arabia*

[3]*School of Pharmacy, The University of Queensland, Australia*

[4]*Centre for Integrated Preclinical Drug Development, The University of Queensland, Australia*

ABSTRACT

Multiple sclerosis (MS) is debilitating disease affecting the central nervous system (CNS). MS pathology has been primarily associated with demyelination and neuroinflammation in the CNS white matter (WM) structures. Recently, clinical studies using high-field magnetic resonance imaging (MRI) have reported diffuse pathological changes observed in the grey matter (GM) regions. This study aims to investigate neurological changes underpinning disease development in mild experimental autoimmune encephalitis (EAE) mouse model of relapsing-remitting MS using magnetic resonance diffusion-weighted imaging (DWI). Relapsing-remitting EAE disease was induced in C57BL/6 mice using myelin oligodendrocyte protein (MOG35-55) emulsified in saponin (Quil-A) adjuvant and pertussis toxin. The animal clinical scores were monitored throughout the disease and prior to fixation at acute and chronic relapsing stages. Ex-vivo brain samples were imaged using conventional MRI and DWI at 16.4 Tesla. MRI relaxation and diffusion tensor imaging (DTI) parameters were evaluated to assess structural changes and the results were correlated with BlackGold II myelin staining. Acute EAE mice showed increases in mean and radial diffusivities within WM structures the corpus callosum, external capsule and hippocampal commissure. Chronic EAE mice showed extensive reductions in fractional anisotropy in vital GM structures such as the motor cortex, somatosensory area, and rostral hippocampal regions, as well as in part of the WM anterior cingulate and external capsule. DTI findings were confirmed by a notable reduction in myelin staining and correlated with adverse clinical scores in chronic animals. This study presented for the first time the use of *ex-vivo* ultra-high-field MRI to detect mild EAE pathology in GM somatosensory and motor cortex using DTI MRI, providing invaluable insight into neuropathological evolution during the relapsing-remitting disease.

KEYWORDS: Magnetic resonance imaging; Diffusion tensor imaging; Multiple sclerosis; Experimental autoimmune encephalomyelitis; Demyelination; Relapsing-remitting; Mouse model; Cortical gray matter; White matter

ABBREVIATIONS: AD: Axial diffusivity; DWI: Diffusion-weighted imaging; DTI: Diffusion Tensor Imaging; EAE: Experimental autoimmune encephalitis; FA: Fractional anisotropy; MD: Mean diffusivity; MRI: Magnetic Resonance Imaging; RD: Radial diffusivity; MS: Multiple Sclerosis; BBB: Blood Brain Barrier; TMEV: Theiler's Murine Encephalomyelitis Virus; EAE: Experimental Autoimmune Encephalomyelitis; CNS: Central Nervous System; CIPDD: Centre for Integrated Preclinical Drug Development; VBM: Voxel Based Morphometry; ROI: Region Of Interest

Quick Response Code:

Address for correspondence: Nyoman D Kurniawan, Centre for Advanced Imaging, The University of Queensland, Australia

Received: March 04, 2021 **Published:** March 16, 2021

How to cite this article: Othman I Alomair, Nematullah Khan, Maree T Smith, Ian M Brereton, Graham J Galloway, Nyoman D Kurniawan. Diffusion Weighted Magnetic Resonance Imaging Revealed Changes in the Somatosensory and Motor Cortex of a Mild Relapsing-Remitting Experimental Autoimmune Encephalitis Mouse Model. 2021- 3(2) OAJBS.ID.000263. **DOI:** 10.38125/OAJBS.000263

INTRODUCTION

The role of magnetic resonance imaging (MRI) has been important in multiple sclerosis (MS) research, has assisted the improvement of diagnostic accuracy and in assessing treatment efficacy in clinical trials. Key aspects of MS that can be monitored by MRI include blood brain barrier (BBB) leakage, inflammation, demyelination/remyelination, axonal injury, and changes in brain connectivity and structural volumes [1-2]. Various experimental animal models have been used to investigate the complex pathobiology of MS [3]. These models usually target a specific aspect of the disease rather than attempting to replicate the full spectrum of human MS. For example, TMEV (Theiler's murine encephalomyelitis virus) has been used to study the effect of viral infection and chronic progression of MS. TMEV can produce a monophasic disease stage (relapsing for seven days and recovery within three weeks) or bi-phasic (mono-phasic with chronic demyelination) [4], where lesions are commonly observed in the spinal cord. However, TMEV model is aggressive and cannot be used to model the early stage of MS during which the relapsing-remitting disease stages occur [5]. Other models, such as toxin-induced demyelination model using either Cuprizone or Lysolecithin, have been developed to specifically investigate the process of demyelination and remyelination rather than the immunopathobiology of MS [6].

Experimental autoimmune encephalomyelitis (EAE) is a classical animal model of MS. EAE is characterized by the development of central nervous system (CNS) neuroinflammation that leads to demyelination and neurodegeneration. To assess sensory deficits in EAE-mice, the immunization protocol can be specifically tailored to produce mild relapsing-remitting (RR) symptoms with partial recovery between relapses [7]. Unlike the conventional EAE model, in which mobility can be severely impaired, this mild EAE model has been developed to study the pathobiology of MS-associated neuropathic pain [7]. Mild EAE mice did not suffer from hind limb paralysis for at least 60 days post-model induction and exhibited brisk hind paw withdrawal in response to applied light touch stimuli [7]. The ability to detect mild EAE pathology in the GM somatosensory cortex using MRI is important, as pain behaviors can now be assessed without confounding motor deficits, providing better insights into neuropathological changes during the relapsing-remitting disease course. In this RR-EAE mice model, the clinical presentation of disease fluctuated with time, providing opportunities for understanding the complex mechanisms of MS in the relapsing-remitting course [7], such as demyelination and axonal damage [8].

Axonal damage has been identified as an early feature of MS; however, this is still a controversy in the literature [1]. Most conventional rodent EAE models primarily exhibit pathology in WM structures. However, MRI methodology to determine whether axonal damage precedes or follows demyelination in RR-EAE is still not established [9]. Establishing a MS animal model with clear pathology in the GM cortical areas is important for understanding MS-related CNS dysfunctions and potentially serves as a platform for establishing new MS imaging biomarkers.

Detection of demyelinated lesions in the cerebral cortex has been integral to the recent study of multiple sclerosis pathology. It has been recognized that demyelination may affect not only the white matter structures, but also in the cortical grey matter and deep grey matter nuclei [10]. In MS patients, the commonly observed cortical lesions are subcortical, perivascular intracortical and subpial, which appear as band and extends to over the adjacent gyri and sulci. The subpial lesions are extensive and can be observed in the cerebrum [11], cerebellum [12], and hippocampus [13]. Cortical lesions are especially interesting because they have been observed during both early [14] and late stages of MS [15]. However, investigation and tracking of these lesions in early-stage relapsing-remitting MS patients were difficult due to limitation of the imaging spatial resolution [16] and accurate diagnosis of the MS onset [3].

Diffusion-weighted MRI (DWI) plays an important role in interpreting processes associated with complex disease mechanisms in MS. Several diffusion parameters can be derived from diffusion tensor imaging (DTI) [17]. These parameters define the dimensions and shapes of the tensor ellipsoid that describes the anisotropy of diffusion. The largest eigenvector ($v1$) and its associated eigenvalue ($\lambda 1$) represent the direction and magnitude of the major diffusion vector and reflect the orientation of the axonal fibre bundle in brain [17]. $v1$ is used in DTI tractography for the reconstruction of the fibretracks. $\lambda 1$ is referred to as the longitudinal or axial diffusivity (AD), which specifies the rate of diffusion along the main diffusion direction. The second ($v2$) and third ($v3$) eigenvectors are orthogonal to the major diffusion direction and their eigenvalues ($\lambda 2$ and $\lambda 3$) provide the diffusion magnitude in the transverse directions. The mean of $\lambda 2$ and $\lambda 3$ is known as the radial diffusivity (RD) [18]. In addition to the axial and radial diffusivities, other rotational invariant diffusion metrics can be derived from the three eigenvalues, which include the mean diffusivity (MD) and the fractional anisotropy (FA). MD describes the average of diffusivity components within each voxel [8]. FA describes the degree of the directionality of the intra-voxel diffusivity and provides a sensitive measure for microscopic changes of diffusion [19].

Several studies [9,20] have reported strong correlations between myelin and axonal integrity with DTI parameters. An increase in MD was suggested as an indicator of inflammation [9]; an increase in RD as an indicator of myelin loss and axonal damage; a decrease in AD has been linked with axonal injury and demyelination [21]; and FA as a marker for demyelination and providing some measures for the integrity of brain white matter connectivity [8]. To-date, there are minimal reports of DTI changes in the EAE mouse brain [9], with most studies focussing on the spinal cord [22] or optical nerve [23-24]. Chronic EAE mice exhibited reduced FA and AD in affected white matter [20,25]. Here we investigate the presence of subtle changes in DTI parameters measured in the brain in our novel mild relapsing remitting EAE mouse model [7] and aim to correlate clinical scores with DTI parameters. This EAE model can potentially reveal subtle development of neurological impairment during the early stage of MS [7,26].

METHODS

All mice were housed and handled in accordance with Queensland Animal Care and Protection Act 2001 and the current NHMRC Australian Code of Practice for the Care and Use of Animals for Scientific Purposes. The use of animals was approved by The University of Queensland's Animal Ethics Committee under the following certificates: CAI/004/11 (Centre for Advanced Imaging) and CIPDD/170/11 (Centre for Integrated Preclinical Drug Development).

EAE Immunization and Study Design

C57BL/6 female mice (4-6 weeks old) were used for induction of mild relapsing-remitting EAE disease using subcutaneous

injection of MOG35-55 (200μg) mixed in saponin adjuvant (Quil-A) (45μg) and two intraperitoneal injections of pertussis toxin (PT) (200-250ng) administered 48h apart [7]. Age-matched mice were used for control groups that consisted of naïve (untreated) and sham mice (receiving only Quil-A adjuvant and pertussis toxin). An additional control group is comprised of 10-12 weeks old naïve control mice. Clinical scoring of EAE-mice was performed using half-point grading scale ranging from 0-4 (arbitrary units, a.u.) [7]. Incidence of EAE-disease was characterized by clinical score of ≥ 1 a.u. as previously shown [7].

EAE-mice were grouped for MRI testing at acute stage (first relapse around day 12-14 post-immunization (p.i.)) and chronic disease stage (a relapse around day 55 p.i.) for comparing the neurobiological changes in brain tissues over the disease course. In both disease stages, EAE mice were tested at score of 1.5 characterized by limp tail and hind limb weakness in comparison to control groups at that time-point.

Sample Preparation

Ex vivo MRI samples were prepared using C57BL6 mice in the following groups: (i) naïve (untreated) mice (*n*=8, 10-12 weeks old); (ii) sham and EAE mice at acute stage (*n*=7/ group, 8-10 weeks old), (iii) sham and EAE mice at the chronic stage (*n*=7-9/ group, 12-14 weeks old). Mice were anaesthetized and transcardially perfused with 0.1M phosphate-buffered solution (PBS) and 4% paraformaldehyde (PFA).

All brain samples were prepared with the same incubation and washing protocol. Following extraction, brain tissues were washed with PBS for 48h prior to MR imaging [27]. The brain samples were then immersed in Fomblin Y06/06 (Solvay Solexis, Italy) to preserve the sample during the overnight imaging acquisition. The scanner room temperature was maintained at 22 °C [28].

MRI Acquisition

MRI samples were prepared, and data acquired without contrast agent using previously published protocols [29]. Imaging was performed using a 16.4T vertical 89 mm-bore microimaging system, running Paravision 5.1 (Bruker Biospin, Karlsruhe, Germany), fitted with a Bruker micro2.5 gradient system and 15mm i.d. SAW microimaging coil (M2M Imaging, Brisbane, Australia).

DWI

3D HARDI data were acquired using the Stejskal-Tanner pulse-field gradient spin echo sequence, with 30 diffusion gradient directions at b=3000 s/mm2, and 2 images with b=0, δ/Δ=2.4/6.4 ms, TR/TE=400/14.5ms, and at 100 μm3 isotropic resolution, the total acquisition time was 14h 44m. DWI spin echoes were zero-filled by a factor of 1.5 prior to Fourier transformation, resulting in 67μm3 isotropic resolution. Diffusion tensor imaging (DTI) parametric maps were calculated using MRtrix program [30] version 0.2.9.

Conventional MRI

1) High-resolution structural images were acquired using 3D Fast Low angle shot (FLASH) and 3D multiple gradient echo (MGE) to produce T1/T2* weighted images.

2) T1 and T2 relaxation times were calculated from 2D Rapid Acquisition with Relaxation Enhancement images with variable TR and TE (RARE VTR).

3) 2D multiple gradient echo (MGE) images were acquired to quantify the T2* relaxation time (Table 1 & 2) for detailed imaging parameters).

Table 1: FA, MD, and RD values of EAE affected areas detected by VBM.

	Controls	Acute Adjuvants	Acute EAE	Chronic Adjuvants	Chronic EAE
FA Anterior Cingulate	0.27 ± 0.07	0.26 ± 0.07	0.26 ± 0.07	0.23 ± 0.07	0.21 ± 0.07
FA Primary and Secondary Motor Cortex	0.25 ± 0.07	0.24 ± 0.06	0.24 ± 0.07	0.22 ± 0.06	0.21 ± 0.06
FA Soma To-Sensory Cortex	0.19 ± 0.06	0.19 ± 0.06	0.18 ± 0.06	0.17 ± 0.05	0.16 ± 0.05
Fa Hippocampus	0.24 ± 0.06	0.24 ± 0.06	0.23 ± 0.06	0.22 ± 0.06	0.21 ± 0.06
MD Corpus Callosum	3.2×10-04 ± 2.69×10-05	3.3×10-04 ± 2.03×10-05	3.4×10-04 ± 2.28×10-05	3.0×10-04 ± 2.67×10-05	2.9×10-04 ± 1.8×10-05
RD Corpus Callosum	2.1×10-04 ± 2.02×10-05	2.3×10-04 ± 1.69×10-05	2.4×10-04 ± 2.28×10-05	2.0×10-04 ± 1.96×10-05	1.9×10-04 ± 1.42×10-05

Note: Values are expressed as mean±SD

Table 2: Summary detection of EAE pathology using MRI.

Brain Structure	ROI Analysis				VBM Analysis			TBSS Analysis		
	FA	MD	RD	T2	FA	MD	RD	FA	MD	RD
Rostral cc		↑	↑			↑	↑		↑	↑
Middle cc		↑	↑	↑		↑	↑		↑	↑
Caudal cc		↑	↑	↑		↑	↑		↑	↑
fmi		↑	↑			↑	↑		↑	↑
fmj		↑	↑			↑	↑			
ec		↑	↑	↑	↓	↑	↑	↓	↑	↑
Rt-cp			↑				↑			↑

Lt cp			↑				↑			↑
Fimbria		↑								↑
Rt-opt			↑				↑			
Lt-opt			↑				↑			
Internal capsule			↑							↓
Rt cingulate	↓			↑	↓			↓	↑	
Lt cingulate	↓			↑	↓			↓	↑	
Rt M cortex	↓			↑	↓			↓		
Lt M cortex	↓			↑	↓			↓		
Rt S cortex	↓			↑	↓					
Lt S cortex	↓			↑	↓					
Rt Hippocampus	↓			↑	↓					
Lt Hippocampus	↓			↑	↓					
Rt caudate putamen				↑						
Lt caudate putamen				↑						

Note: Chronic EAE mice have higher T2 and lower FA in comparison to control mice, whereas acute EAE mice have lower MD and RD in comparison to chronic EAE mice.

Image Registration

For spatial normalization, a study-specific b0 (image acquired without diffusion gradient) and FA map templates were created from initial brain sample cohorts (n=28) using an iterative group-wise diffeomorphic normalization procedure (SyN) as implemented in buildtemplateparallel.sh script v0.0.13 of the program Advanced Normalization Tools (ANTs v1.9.x, picsl.upenn.edu/software/ants/) [31]. All individual data were registered to the template using FMRIB's Linear and Non-Linear registration tools (FLIRT/FNIRT, fsl.fmrib.ox.ac.uk) [32].

Linear Registration

The following parameters were used during linear registration: cost function = normalized correlation for intra model registration; full orientation and angular alignment search in X, Y and Z-axes; 3D affine registration with 12 degrees of freedom; trilinear interpolation method. The interpolation is part of the final transformation and not part of registration tool [33].

Non-Linear Registration

The following parameters were used for FNIRT three-step registration: A) a gradual decrease of subsampling factors from 4, 2, and 1, in which the registrations were initially done at coarse resolution and increasing to the full resolution at the last iteration. B) A gradual decrease in the level of image smoothing at 0.3, 0.15, and 0 mm for the input and reference images, where the final registration step is done without smoothing. C) Warp field resolutions of 1, 1, 1 mm which specify the position of the points of displacement fields. D) Bias field resolutions, used to control the sensitivity to image bias that can vary gradually over the space, was set to 5x the warp field resolution. E) Lambda, which is used to smooth the warp field to the reference image and control how much smoothing affects the input image, was set to 30, 15 and 4. Lambda values have to be selected carefully to match the type of data. F) The number of iterations for each step was set to 5, 5, 5, to reach a compromise between the accuracy of the registration and the length of registration protocol. G) Intensity modeling was used for the initial two steps, and none was used for the final registration step. H) Masks were applied in both reference (template) and input image to help registration. The MD, AD and RD maps were then shadow registered to the mouse brain template using FSL applywarp command. The Jacobian (tissue displacement) map from each sample was produced during FNIRT registration of 3D ex vivo b0 DWI to the template image.

Data Analysis

After registration of individual data to the template, analyses were performed using three approaches: region of interest (ROI) based analysis [34], voxel-based morphometry (VBM) [35] and tract based spatial statistics (TBSS) [36].

Initial ROI-based analyses used only WM structures because they are well distinguished in the FA maps and they were known to be susceptible to pathological changes in the EAE model. Twelve WM ROIs: forceps minor (fmi), major (fmj), rostral (R-cc), middle (M-cc) and caudal (C-cc) corpus callosum, external capsule (ec), hippocampal fimbria (fi), right and left of cerebral peduncles (Rt-cp and Lt-cp), right and left of optic tracts (Rt-opt and Lt-opt), and internal capsule (ic) were drawn manually on the FA template using ITK-snap (Figure 1), using C57 adult brain histology atlas as reference [37]. DTI parametric values were measured after inverse registrations of the ROIs from the template to individual samples [38].

For 2D T1, T2 and T2* maps, accurate registration was difficult to obtain due to large slice thickness compared to in-plane resolution and variations in slice position. For these datasets, ROIs were drawn manually on single slices and matched to the same anatomical structures in all mouse groups (Figure 1).

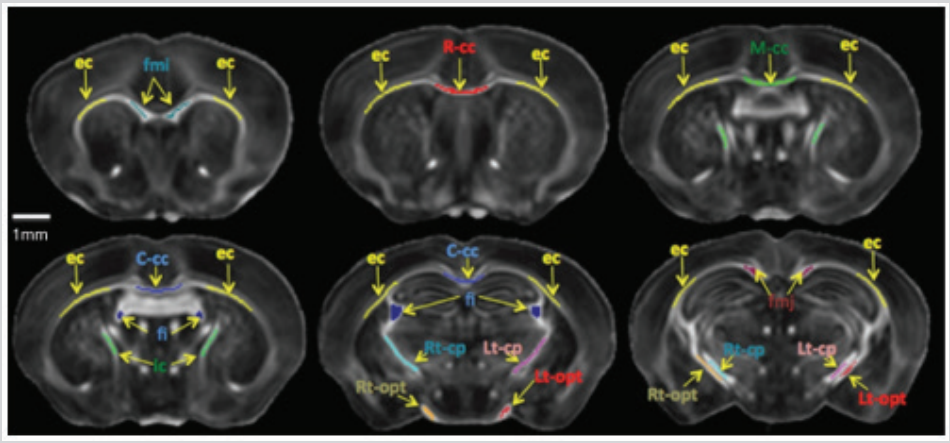

Figure 1: WM structures segmented for ROI-based analyses. ROIs were drawn manually in the center of WM structures on the FA map template using an ITK-snap. The corpus callosum (CC) was divided into five segments, including forceps minor (fmi, light blue) and major (fmj, red), rostral (R-cc, red) middle (M-cc, green) and caudal (C-cc, bottom). Other WM structures examined included the external capsule (ec, yellow), fimbria (fi, dark blue), right (Rt-cp, light blue) and left (Lt-cp, light red) cerebral peduncles (cp), right (Rt-opt, dark yellow) and left (Lt-opt, red) optic tracts, and internal capsule (ic).

Voxel Based Morphometric (VBM) Analysis: DTI parametric maps were analyzed using Statistical Parametric Mapping program (SPM5, www.fil.ion.ucl.ac.uk/spm/). Student t-tests were performed using False Discovery Rate (FDR) correction and $p<0.05$ thresholds for statistical significance. Using the same method, the Jacobian determinant maps were analyzed to determine the presence of brain atrophy. **Tract Based Spatial Statistics (TBSS):** In order to accommodate mouse brain data in FSL TBSS pipeline [36] without changing the code extensively, the resolution specified in the mouse data header was changed to 1mm3 and the FA template was used as the target for TBSS registrations. The FA threshold used to calculate the WM skeleton was > 0.2 in order to exclude the GM and CSF and to include the WM structures (WM FA is in range of 0.35 to 0.8, Figure 2). This threshold is also chosen to prevent analysis in areas with low FA value such as the cortex [39]. Inter-group comparisons were performed between the five animal groups. Voxelwise statistics of the skeletonized FA, AD, RD and MD data were calculated using FSL randomize tool with a threshold for statistical significance $p<0.05$ [40].

Histology

Black Gold II (BGII) myelin staining [41] was used to visualize myelinated axons to confirm the MRI observations. Brain samples (total $n=10$) were sectioned at 50µm slice thickness, using a Leica VT1000s vibrotome (Leica, Germany) and the sections were then stored at 4 °C in PBS until staining.

RESULTS

ROI-Based Analyses of Diffusivity and MR Relaxation

DTI parameters ROI based analyses of FA revealed no significant difference between all mouse groups (Figure 2). However, increases in MD in WM structures including the corpus callosum segments and the external capsule were observed in the acute group (Figure 3). AD values were generally higher in the acute EAE group compared to the chronic group, particularly in the caudal and forceps minor corpus callosum. Chronic EAE mice exhibited lower AD in the forceps major corpus callosum, external capsule and fimbria hippocampus (Figure 4). RD values were also generally higher in the acute mice compared to chronic groups in WM structures such as the corpus callosum segments, external capsule, cerebral peduncles, optic tracts, and internal capsule (Figure 5).

T1, T2 and T2* relaxation times. T1 relaxation times were variable among the studied groups with no significant differences detected between groups (Figure 6). T2 relaxation times were significantly increased in chronic EAE mice compared to controls and to acute EAE group. This was observed in the cingulate cortex, motor areas, somatosensory areas, hippocampus, and caudate putamen (Figure 7). The decrease of FA appears to be inversely correlated with the increase in T2 relaxation times. There was no significant difference in T2* relaxation times observed between the groups (Figure 8). The absence of changes detected by 2D T1 and T2* parameters were confirmed with a whole brain VBM analysis of 3D T1 and T2*-weighted images. There was no evidence for regional volumetric changes as tested using VBM of the Jacobian determinants of 3D T1 weighted data.

Whole-Brain Analyses of Diffusivity

Unlike in MRI presentations of human MS, there were no detectable lesions in any stage of the disease in RR EAE mice. Acute EAE mice have elevated MD and RD compared to chronic EAE mice. VBM and TBSS analyses of MD (Figure 2 & 3) and of RD (Figure 4 & 5) between these groups showed increases in various regions of the corpus callosum, external capsule and in fimbria. Compared to MD, VBM analysis of RD detected additional changes in the internal capsule, cerebral peduncles, and optic tracts, whereas TBSS detected additional changes in the anterior commissure and the internal capsule.

There was no significant change detected in AD using VBM and TBSS between the controls and EAE animals at the acute and chronic stages. Chronic brain pathological changes were observed by VBM comparison between naïve control and chronic EAE-mice (Figure 6). The reduction of FA revealed by VBM was prominent in GM brain areas including the motor cortex, primary somatosensory cortex, anterior cingulate and rostral CA1 (cornu ammonis) of the hippocampus; and in the WM external capsule and parts of the forceps minor of the corpus callosum. TBSS (Figure 7 & 8) revealed

similar changes to VBM, however, GM changes were unmeasured as TBSS analyses were limited to FA projected to the skeleton of WM structures [36]. The decrease of FA appears to be inversely correlated with the increase in T2 relaxation times. Table 1 contains FA values, MD and RD of regions showing significant changes. MRI parametric changes detected in this mild RR *ex-vivo* EAE mouse brain study is summarized in Table 2.

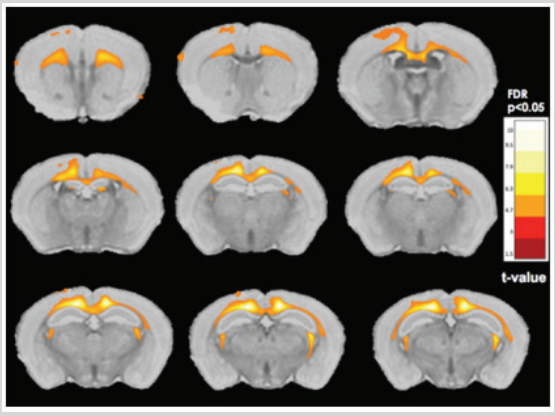

Figure 2: VBM analysis of MD map shows extensive MD elevation in acute EAE mice. The hot colour map shows t-statistics and represents areas with significantly increased MD in the acute EAE mice compared with chronic EAE (*p*-value<0.05).

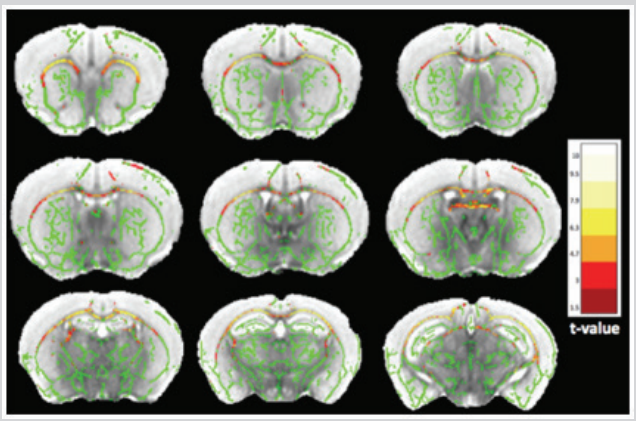

Figure 3: TBSS analysis of MD maps of acute versus chronic EAE mice (axial view). The FA-derived WM skeleton is shown in green. The hot colour map shows t-statistics and represents areas with significant MD increase in the acute EAE mice comparing with chronic EAE (*p*-value< 0.05).

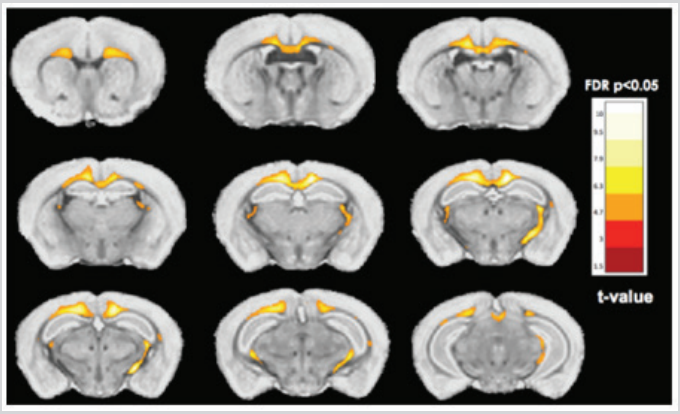

Figure 4: VBM analysis of RD map shows extensive RD elevation in the acute EAE mice. The hot colour map shows t-statistics and represents areas of significantly increased RD in the acute EAE mice compared with chronic EAE (*p*-value<0.05).

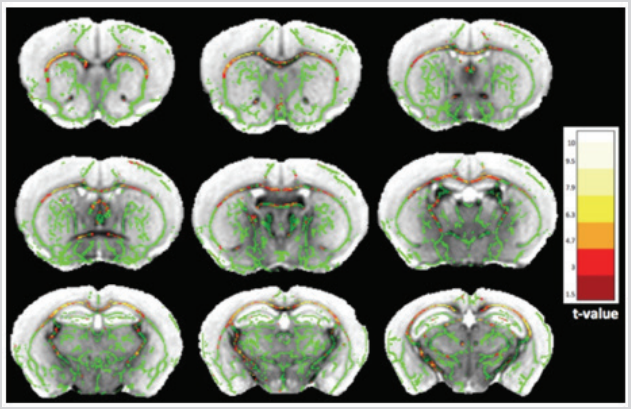

Figure 5: TBSS analysis of RD maps of acute versus chronic EAE mice (axial view). The WM skeleton is shown in green. The hot colour map shows t-statistics and represents areas with significantly increased RD in the acute EAE mice comparing with chronic EAE (p-value< 0.05).

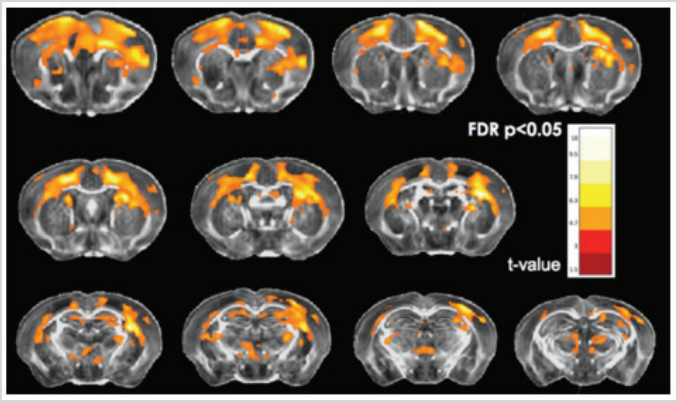

Figure 6: VBM analysis of FA map shows extensive FA reduction in the chronic EAE. The hot colour map shows t-statistics and represents areas with significant FA reduction in the chronic EAE mice (p-value<0.05).

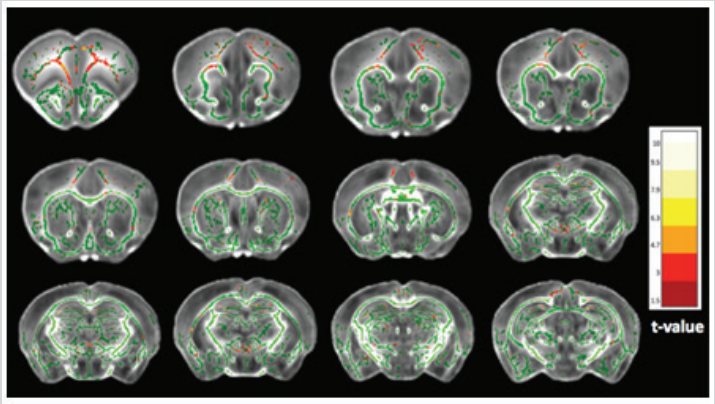

Figure 7: TBSS analysis of FA maps of controls subjects versus chronic EAE mice (axial view). FA (WM) skeleton of the template is shown in green. The hot colour map shows t-statistics and represents areas with significant FA reduction in the chronic EAE mice (*p*-value<0.05).

Detection of Demyelination Using BGII Staining

BG myelin staining revealed significant reductions in the coherence of myelin fibres in cortical areas, including the anterior cingulate cortex, somatosensory areas, and primary motor areas (Figure 9). These histological changes can be mapped to areas with FA reductions in chronic EAE mice as shown by VBM and TBSS analysis. There was no significant reduction of myelin fibres detected in the acute adjuvant, EAE and chronic adjuvant groups.

DISCUSSION

Neuropathological changes in mild RR-EAE mice were detected using 16.4T high-resolution ex-vivo diffusion-based MRI studies.

In the acute stage, increases in diffusivity parameters MD and RD were detected in major WM structures. In the chronic stage, these changes were no longer detectable. Instead, there was a reduction in FA accompanied by increases in T2 relaxation both in the WM and GM structures. Histology revealed demyelination in chronic but not in acute mice affecting both gray and white matter structures.

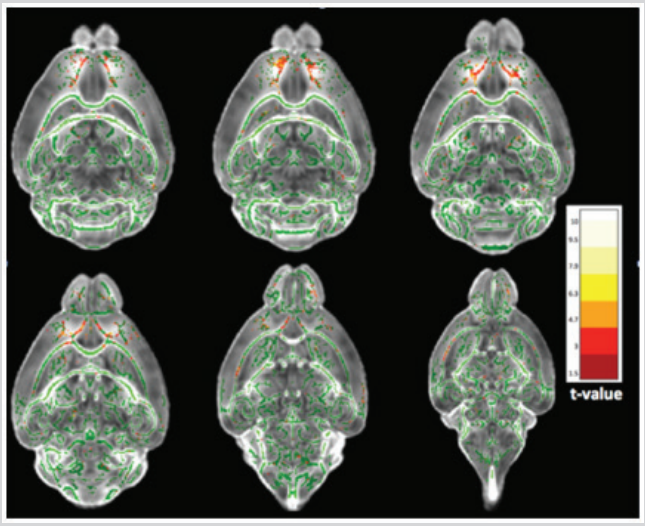

Figure 8: TBSS analysis of FA maps of controls subjects versus chronic EAE mice (sagittal view). The FA (WM) skeletons are shown in green. The hot colour map shows t-statistics and represents areas with significant FA reduction in the chronic EAE mice (*p*-value<0.05).

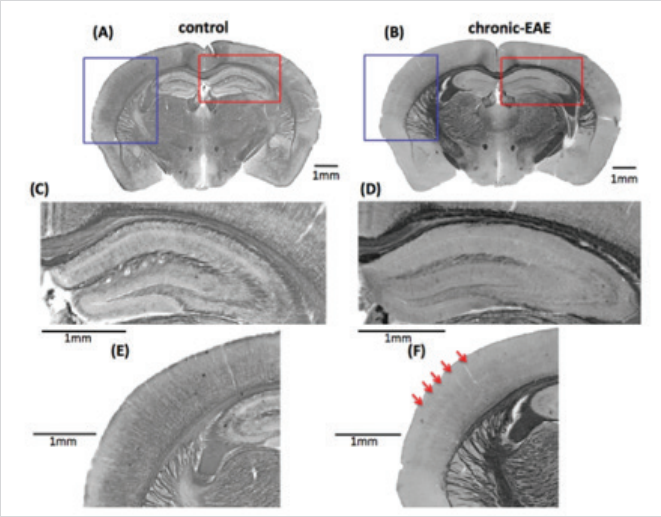

Figure 9: Comparison of BG myelin stains obtained for control (A) and (B) chronic-EAE mice. Zoomed regions (red boxes) of the hippocampus in control subject (C) and (D) chronic-EAE showing extensive reduction of myelin stain intensity in this area. Zoomed regions (blue boxes) of the somatosensory areas of the control (E) and chronic-EAE (F) respectively, red arrows point to the area of extensive reduction of myelin fibre staining.

Acute Stage Neuro-Inflammatory Changes in RR EAE

MRI data acquisition of the acute group was performed immediately at the first relapsing period. As there was no demyelination or atrophy detected, the increase of MD and RD values may be primarily attributed to inflammation processes. DTI changes in this group appeared transient and no longer observed in the chronic stage. Besides inflammation, subtle axonal injury may also occur which then partially recovered through neuroprotection, resulting in normal appearing white matter [42]. This diffusivity changes in the acute group appeared to be similar to that detected in proteolipid protein (PLP) induced RR-EAE model. At the end of the RR cycle, PLP RR-EAE mice showed substantial remyelination as indicated by the recovery of myelin MRI magnetization transfer signal and myelin basic protein staining [9].

Chronic Stage Neuro-Inflammatory Changes in RR EAE

Using littermates of mice examined in this study, Khan et al showed that chronic mild RR-EAE mice also exhibited classical MS-like neuro and immunopathology characteristics, such as activation of glial cells and astrocytes, T-cell infiltration and strong demyelination in the brain and lumbar spinal cord [7]. In the corpus callosum there was an approximately ~40% reduction of myelin in chronic EAE, and there were approximately 3- and 5-fold increases

in astrocyte and microglia activations compared to naïve control animals, respectively. Chronic sham animals appeared to have a small decrease in myelin content and small increases in astrocytes and microglia activation compared to naïve control animals, but these changes were not statistically significant.

These observations support the DTI finding of extensive FA reductions in important primary and secondary motor, somatosensory cortical areas. FA changes were corroborated with BG myelin staining showing co-localization of areas with demyelination. Our finding also supports a previous study which shows that FA were correlated to the amount of myelin in neurological tissue [43]. The development of neurological disabilities in the chronic EAE groups may be linked to extensive demyelination in the motor and sensory cortical areas.

In neuronal tissues, the myelin sheath and axonal membrane are tightly coupled in terms of structural and functional properties. Both neuronal structures act as barriers to water diffusion along the perpendicular axis of the axon [44]. It is often difficult to distinguish between axonal and myelin sheath injuries using diffusion tensor MRI because damage of one lead to damage of the other [8]. The cytoskeletal architecture inside the axon would also contribute to water diffusion parallel or perpendicular in the axon [44].

DWI experiments typically measure diffusion of water from both the intracellular (inside the axonal environment) and extracellular components (among axons) [45]. Both DWI sequence parameters and tissue microstructure contribute significantly to the sensitivity of DTI derived parameters as surrogate biomarkers in detecting pathological changes. In addition, there is no simple animal model that can produce pure axonal or myelin pathologies [8,44].

To interpret the conventional DTI derived parameters, it can be assumed that WM signals contain signal contributions from normal or abnormal tissues without considering fibre crossings. There are several scenarios that could be used to describe changes in the DTI derived parameters:

1) Decreasing AD and increasing RD can be correlated with significant axonal injuries and demyelination. This correlation was established previously in CNS injury rodent models [46].

2) When inflammation is present due to axon and myelin injury, cell proliferation (increased presence of oligodendrocytes, astrocytosis, microgliosis, or other immune cells) between the axon fibres will produce a stronger inhibition of axial diffusion of water. This situation would result in a large decrease in AD and a smaller decrease in RD. In this scenario, the DTI parameters may underestimate the extent of demyelination and overestimate the extent of axonal injury. The increase in cellularity will increase the presence of highly restricted intracellular diffusion [47].

Our chronic RR EAE model appeared to correlate with this scenario, in which decreases in both AD and RD were observed. However, it could also be a pseudo-normalization process due to the fluctuation of the disease cycle. To better validate this scenario, additional histology data would be required, such as axon neurofilament staining and microglia staining in addition to the data available for the validation of demyelination using BG myelin staining.

3) Major axonal loss is usually observed in the chronic MS disease stage, which leads to the increase in RD, but AD remained unchanged due to the increase in isotropic diffusion components [48].

4) The interpretation of DTI derived parameters becomes more complicated if there is coexistence of cellular infiltration, demyelination, significant axonal loss and axonal injury [49].

In our experiment, we have observed an increase in RD in most of the WM structures in acute EAE compared to chronic EAE and naïve controls. The AD values of the acute groups did not decrease which could be interpreted as the presence of inflammation without demyelination after the first relapsing cycle. T2 relaxation appeared to be more sensitive, compared to T1 and T2*, in measuring the pathological changes. Areas with increased T2 relaxation are co-localized with areas with decreased FA. One cuprizone study suggested that there was a correlation between the increase of T2 relaxation and demyelination, and that inflammatory cellular infiltration might have contributed to T2 signal abnormalities [50].

Detection of Cortical GM Changes

This study used both ANTs diffeomorphic registration with VBM [51] and TBSS [52] for detecting changes in DTI parameters. Recently it was reported that the ANTs-VBM method outperformed TBSS due to a more accurate registration [53]. Our results showed that ANTs-VBM was more sensitive in detecting distinct FA reductions in the chronic RR-EAE mouse cortical and gray matter areas compared to TBSS. This difference may be due to the limitation of TBSS, as cortical and gray matter areas have low anisotropy (FA≤0.2), which is below TBSS thresholds required for the projection of neighboring FA voxels to the skeletonized WM tracts. For areas with higher FA, such as the anterior cingulate cortex, VBM and TBSS reported similar change.

EAE and MS Cortical Demyelination

Our chronic RR EAE mice exhibited FA reduction in cortical areas layers I-III, similar to pattern of cortical demyelination in MS human brain [54]. Cortical demyelination has also been observed in rats induced with focal EAE, in which the pathology resolved relatively rapidly, reflecting the capability of cortical regions to remyelinate [55]. GM lesions are different to WM lesions, in which the lymphocyte infiltration is absent (with exception of some activated microglia) and BBB disruption level is low [56]. GM lesions are usually characterized by a low degree of inflammation, demyelination and neuronal and glial synaptic loss, axonal loss and microglial proliferation [54]. It was suggested that FA decrease may be related to the local activation of microglial cells [56]. Demyelination in the chronic EAE model was accompanied by the presence of activated microglia and astrocytes. Somatosensory cortical demyelination observed could be contributing factors to increased mechanical allodynia reported in this parallel study [7].

Recent studies described strong correlations between GM lesion and clinical disability in MS patients [57]. Cortical demyelination may have occurred during the early relapsing-remitting stage, and in some cases, it occurred prior to development of focal WM lesions. These lesions accumulate over time and the chance of detection increase dramatically. Human MS cortical lesions are typically difficult to detect using MRI, but they have been extensively observed in several post-mortem studies. The development of the double inversion recovery sequence for clinical imaging at high magnetic field (7 Tesla) has facilitated detection of these lesions in MS patients [58].

A three-year follow up case study found that FA values were increased in cortical lesions and normal appearing gray matter in RRMS patients compared with control subjects [59]. However,

a more recent DTI study showed a decrease in FA values in cortical lesions and the normal appearing cortex of MS patients. These variations in FA characteristics are thought to be useful to distinguish MS phenotypes: benign MS, RRMS and SPMS [60].

In our model, extensive FA reductions were observed in cortical areas, and validated with BG myelin staining as areas with extensive demyelination. The major differences between our experiment and the Calabrese et al study highlights the complexity of MS in humans because the disease can originate from various spontaneous processes such as axonal injury and breaking of the blood brain barrier, whereas EAE induced in mice is caused by immunoreaction to brain tissue antigens. In humans, the cortical areas are highly prominent and occupy a larger volume compared to the rodent brains [56].

Several human and rodent imaging studies have revealed that pain can originate from multiple areas of the brain [61]. Our model has been initially designed to understand pain mechanisms in MS [62]. In our experimental model, we have observed significantly reduced FA values in the anterior cingulate (acc) areas. This region is functionally heterogeneous. In rodent brain it is correlated with several cognitive tasks which include attention [63], motor (e.g. preparation and execution of movement) [64] and sensory (e.g. pain) [65]. A recent study [66] also revealed the role of the acc in remote spatial or non-spatial memory. The presence of demyelinated axons in this area is thought to cause functional disruption and the development of neuropathic pain [62].

The somatosensory cortex has been associated with discriminative aspects of the pain experience, for example, the location, duration and intensity of harmful stimulus [67]. At the end of the relapsing-remitting cycle, the reduction of FA due to demyelination in these areas may be responsible for the development of mechanical allodynia (pain sensitivity). Additionally, neuroinflammation in the CNS may result in increased hind paw hypersensitivity in these RR EAE mice [62].

MS may affect each patient differently and different regions of the CNS may be affected more extensively in some patients than others [68]. For example, some patients may experience sensory and motor disability due to lesions in the spinal cord. However, other patients may have cognitive impairment due to extensive cortical lesions [56]. Establishing animal models which affect or target specific areas could be advantageous for a better understanding of MS development in these regions [69].

Also, this may assist in the discovery of neuroprotective treatments for specific CNS regions because each region is known to vary in response to neurotrophic factors, receptor expression and sensitivity to excitotoxic-induced cell death [70]. In our experimental MS model, cortical areas are extensively affected. Therefore, a treatment may be tailored to target these CNS regions specifically [69].

SUMMARY

DTI parameters are sensitive to differences in neuropathology between the acute and chronic stages in a mild RR-EAE mouse model of neuropathic pain. In the acute stage, increases in MD and RD parameters were observed, but these were not accompanied by demyelination, suggesting the presence of characteristic inflammatory reactions. These increases in diffusivities were no longer observed in the chronic EAE mice. Instead, extensive FA reductions were detected in WM and GM structures, which were confirmed for demyelination using histology. Important changes were detected in the anterior cingulate cortex, somatosensory and primary motor areas, which may be correlated with increased clinical disability and hypersensitivity in these chronic EAE mice.

ACKNOWLEDGEMENT

We acknowledge the supports from the Queensland NMR Network and the National Imaging Facility (a National Collaborative Research Infrastructure Strategy capability) for the operation of 16.4T MRI at the Centre for Advanced Imaging, the University of Queensland.

REFERENCES

1. Lassmann H (2013) Pathology and disease mechanisms in different stages of multiple sclerosis. J Neurol Sci 333(1-2): 1-4.
2. Alomair OI, Smith MT, Brereton IM, Galloway GJ, Kurniawan ND, et al. (2014) Current developments in MRI for assessing rodent models of multiple sclerosis. Future Neurology 9(4): 487-511.
3. Robinson AP, Harp CT, Noronha A, Miller SD (2014) Chapter 8 - The experimental autoimmune encephalomyelitis (EAE) model of MS: utility for understanding disease pathophysiology and treatment. In: douglas SG, editor. Handb Clin Neurol 122: 173-189.
4. Nelson A, Bieber A, Rodriguez M (2004) Contrasting murine models of MS. Int MS J 11(3): 95-99.
5. Johnson HL, Jin F, Pirko I, Johnson AJ (2013) Theilers murine encephalomyelitis virus as an experimental model system to study the mechanism of blood-brain barrier disruption. J neurovirol: 1-6.
6. Kipp M, Clarner T, Dang J, Copray S, Beyer C, et al. (2009) The cuprizone animal model: new insights into an old story. Acta neuropathol 118(6): 723-736.
7. Khan N, Woodruff TM, Smith MT (2014) Establishment and characterization of an optimized mouse model of multiple sclerosis-induced neuropathic pain using behavioral, pharmacologic, histologic and immunohistochemical methods. Pharmacology Biochemistry and Behavior 126(0): 13-27.
8. Zhang J, Aggarwal M, Mori S (2012) Structural insights into the rodent CNS via diffusion tensor imaging. Trends in neurosciences 35(7): 412-421.
9. Aharoni R, Sasson E, Blumenfeld KT, Eilam R, Sela M, et al. (2013) Magnetic resonance imaging characterization of different experimental autoimmune encephalomyelitis models and the therapeutic effect of glatiramer acetate. Experimental Neurology 240(0): 130-144.
10. Lassmann H (2012) Cortical lesions in multiple sclerosis: inflammation versus neurodegeneration. Brain 135(10): 2904-2905.
11. Kutzelnigg A, Lucchinetti CF, Stadelmann C, Bruck W, Rauschka H, et al. (2005) Cortical demyelination and diffuse white matter injury in multiple sclerosis. Brain 128(11): 2705-2712.
12. Kutzelnigg A, Faber RJC, Bauer J, Lucchinetti CF, Sorensen PS, et al. (2007) Widespread demyelination in the cerebellar cortex in multiple sclerosis. Brain pathology 17(1): 38-44.
13. Geurts JJ, Bö L, Roosendaal SD, Hazes T, Daniëls R, et al. (2007) Extensive hippocampal demyelination in multiple sclerosis. J Neuropathol Exp Neurol 66(9): 819-827.
14. Lucchinetti CF, Popescu BF, Bunyan RF, Moll NM, Roemer SF, et al. (2011) Inflammatory cortical demyelination in early multiple sclerosis. New England J Medicine 365(23): 2188-2197.
15. Magliozzi R, Howell O, Vora A, Serafini B, Nicholas R, et al. (2007) Meningeal B-cell follicles in secondary progressive multiple sclerosis associate with early onset of disease and severe cortical pathology. Brain 130(4): 1089-1104.

16. Tallantyre EC, Morgan PS, Dixon JE, Radaideh A, Brookes MJ, et al. (2010) 3 Tesla and 7 Tesla MRI of multiple sclerosis cortical lesions. J Magnetic Resonance Imaging 32(4): 971-977.

17. Winston GP (2012) The physical and biological basis of quantitative parameters derived from diffusion MRI. Quant Imaging Med Surg 2(4): 254-265.

18. Stieltjes B, Brunner RM, Fritzsche KH, Laun FB (2013) Introduction to diffusion imaging. diffusion tensor imaging: Springer Berlin Heidelberg: 5-40.

19. Aung WY, Mar S, Benzinger TL (2013) Diffusion tensor MRI as a biomarker in axonal and myelin damage. Imaging Med 5(5): 427-440.

20. Sun S, Liang HF, Schmidt RE, Cross AH, Song SK, et al. (2007) Selective vulnerability of cerebral white matter in a murine model of multiple sclerosis detected using diffusion tensor imaging. Neurobiol Dis 28(1): 30-38.

21. Klawiter EC, Schmidt RE, Trinkaus K, Liang HF, Budde M, et al. (2011) Radial diffusivity predicts demyelination in *ex vivo* multiple sclerosis spinal cords. Neuroimage 55(4): 1454-1460.

22. Wang X, Cusick MF, Wang Y, Sun P, Libbey JE, et al. (2014) Diffusion basis spectrum imaging detects and distinguishes coexisting subclinical inflammation, demyelination and axonal injury in experimental autoimmune encephalomyelitis mice. NMR Biomed 27(7): 843-852.

23. Chiang CW, Wang Y, Sun P, Lin TH, Trinkaus K, et al. (2014) Quantifying white matter tract diffusion parameters in the presence of increased extra-fiber cellularity and vasogenic edema. Neuroimage 101: 310-319.

24. Herrera SL, Palmer VL, Whittaker H, Smith BC, Kim A, et al. (2014) Damage to the optic chiasm in myelin oligodendrocyte glycoprotein-experimental autoimmune encephalomyelitis mice. Magnetic resonance insights 7: 23-31.

25. Zhang J (2010) Diffusion tensor imaging of white matter pathology in the mouse brain. Imaging 2(6): 623-632.

26. Khan N, Smith MT (2013) Multiple sclerosis-induced neuropathic pain: pharmacological management and pathophysiological insights from rodent EAE models. Inflammopharmacology 22(1): 1-22.

27. Calamante F, Tournier JD, Kurniawan ND, Yang Z, Gyengesi E, et al. (2012) Super-resolution track-density imaging studies of mouse brain: Comparison to histology. NeuroImage 59(1): 286-296.

28. Benveniste H, Blackband S (2002) MR microscopy and high-resolution small animal MRI: applications in neuroscience research. Prog Neurobiol 67(5): 393-420.

29. Kurniawan ND, Richards KL, Yang Z, She D, Ullmann JF, et al. (2014) Visualization of mouse barrel cortex using *ex-vivo* track density imaging. Neuroimage 87: 465-475.

30. Tournier JD, Calamante F, Connelly A (2012) MRtrix: Diffusion tractography in crossing fibre regions. International J Imaging Systems and Technology 22(1): 53-66.

31. Avants BB, Tustison N, Song G (2009) Advanced normalization tools (ANTS). Insight J.

32. Jenkinson M, Beckmann CF, Behrens TE, Woolrich MW, Smith SM, et al. (2012) FSL. Neuroimage 62(2): 782-790.

33. Greve DN, Fischl B (2009) Accurate and robust brain image alignment using boundary-based registration. Neuroimage 48(1): 63-71.

34. Cercignani M (2010) Strategies for patient-control comparison of diffusion MR data. Diffusion MRI: Theory, Methods, and Applications: 485-499.

35. Whitwell JL (2009) Voxel-based morphometry: an automated technique for assessing structural changes in the brain. J Neurosci 29(31): 9661-9664.

36. Smith SM, Jenkinson M, Johansen BH, Rueckert D, Nichols TE, et al. (2006) Tract-based spatial statistics: voxelwise analysis of multi-subject diffusion data. Neuroimage 31(4): 1487-1505.

37. Paxinos G (2004) The mouse brain in stereotaxic coordinates: Academic press.

38. Yushkevich PA, Piven J, Hazlett HC, Smith RG, Ho S, et al. (2006) User-guided 3D active contour segmentation of anatomical structures: significantly improved efficiency and reliability. Neuroimage 31(3): 1116-1128.

39. Sierra A, Laitinen T, Lehtimäki K, Rieppo L, Pitkänen A, et al. (2011) Diffusion tensor MRI with tract-based spatial statistics and histology reveals undiscovered lesioned areas in kainate model of epilepsy in rat. Brain Struct Funct 216(2): 123-135.

40. Winkler AM, Ridgway GR, Webster MA, Smith SM, Nichols TE, et al. (2014) Permutation inference for the general linear model. Neuroimage 92(100): 381-397.

41. Schmued L, Bowyer J, Cozart M, Heard D, Binienda Z, et al. (2008) Introducing black gold II, a highly soluble gold phosphate complex with several unique advantages for the histochemical localization of myelin. Brain Research 1229: 210-217.

42. Ceccarelli A, Bakshi R, Neema M (2012) MRI in multiple sclerosis: a review of the current literature. Current Opin Neurol 25(4): 402-409.

43. Arnold DL, Dalton CM, Schmierer K, Pike GB, Miller DH, et al. (2013) Imaging of demyelination and remyelination in multiple sclerosis. myelin repair and neuroprotection in multiple sclerosis: 233-253.

44. Beaulieu C (2002) The basis of anisotropic water diffusion in the nervous system - A technical review. NMR Biomed 15(7-8): 435-455.

45. Le Bihan D (2014) Diffusion MRI: what water tells us about the brain. EMBO Molecular Medicine: 1215-1357.

46. Xie M, Tobin JE, Budde MD, Chen CI, Trinkaus K, et al. (2010) Rostrocaudal analysis of corpus callosum demyelination and axon damage across disease stages refines diffusion tensor imaging correlations with pathological features. J Neuropathol Exp Neurol 69(7): 704-716.

47. Sun S, Liang H, Trinkaus K, Cross AH, Armstrong RC, et al. (2006) Noninvasive detection of cuprizone induced axonal damage and demyelination in the mouse corpus callosum. Magn Reason Med 55(2): 302-308.

48. Kim JH, Budde MD, Liang HF, Klein RS, Russell JH, et al. (2006) Detecting axon damage in spinal cord from a mouse model of multiple sclerosis. Neurobiol Dis 21(3): 626-632.

49. Wang Y, Wang Q, Haldar JP, Yeh FC, Xie M, et al. (2011) Quantification of increased cellularity during inflammatory demyelination. Brain 134(12): 3590-3601.

50. Wu QZ, Yang Q, Cate HS, Kemper D, Binder M, et al. (2007) MRI identification of the rostral-caudal pattern of pathology within the corpus callosum in the cuprizone mouse model. J Magn Reson Imaging 27(3): 446-453.

51. Avants BB, Yushkevich P, Pluta J, Minkoff D, Korczykowski M, et al. (2010) The optimal template effect in hippocampus studies of diseased populations. Neuroimage 49(3): 2457-2466.

52. Smith SM, Johansen BH, Jenkinson M, Rueckert D, Nichols TE, et al. (2007) Acquisition and voxelwise analysis of multi-subject diffusion data with tract-based spatial statistics. Nat Protoc 2(3): 499-503.

53. Schwarz CG, Reid RI, Gunter JL, Senjem ML, Przybelski SA, et al. (2014) Improved DTI registration allows voxel-based analysis that outperforms tract-based spatial statistics. Neuroimage 94: 65-78.

54. Geurts JJ, Barkhof F (2008) Grey matter pathology in multiple sclerosis. Lancet Neurol 7(9): 841-851.

55. Merkler D, Ernsting T, Kerschensteiner M, Brück W, Stadelmann C, et al. (2006). A new focal EAE model of cortical demyelination: Multiple sclerosis-like lesions with rapid resolution of inflammation and extensive remyelination. Brain 129(8):1972-1983.

56. Stadelmann C, Wegner C, Bruck W (2011) Inflammation, demyelination, and degeneration, A recent insights from MS pathology. Biochim Biophy Acta 1812(2):275-282.

57. Honce JM (2013) Gray matter pathology in MS: Neuroimaging and clinical correlations. Mult Scler Int 2013: 1-16.

58. Pitt D, Boster A, Pei W, Wohleb E, Jasne A, et al. (2010) Imaging cortical lesions in multiple sclerosis with ultra-high-field magnetic resonance imaging. Arch Neurol 67(7): 812-818.

59. Calabrese M, Rinaldi F, Seppi D, Favaretto A, Squarcina L, et al. (2011) Cortical diffusion-tensor imaging abnormalities in multiple sclerosis: a 3-year longitudinal study. Radiology 261(3): 891-898.

60. Filippi M, Preziosa P, Pagani E, Copetti M, Mesaros S, et al. (2013) Microstructural magnetic resonance imaging of cortical lesions in multiple sclerosis. Mult Scler J 19(4): 418-426.

61. Lee M, Tracey I (2013) Imaging pain: a potent means for investigating pain mechanisms in patients. Br J Anaesth 111(1): 64-72.

62. Khan N, Woodruff TM, Smith MT (2014) Establishment and characterization of an optimized mouse model of multiple sclerosis-induced neuropathic pain using behavioral, pharmacologic, histologic and immunohistochemical methods. Pharmacol Biochem Beh 126: 13-27.

63. Miller EK (2000) The prefontral cortex and cognitive control. Nat Rev Neurosci 1(1): 59-65.

64. Paus T (2001) Primate anterior cingulate cortex: where motor control, drive and cognition interface. Nat Rev Neurosci 2(6): 417-424.

65. Zhuo M (2005) Targeting central plasticity: a new direction of finding painkillers. Curr Pharm Des 11(21): 2797-2807.

66. Teixeira CM, Pomedli SR, Maei HR, Kee N, Frankland PW, et al. (2006) Involvement of the anterior cingulate cortex in the expression of remote spatial memory. J Neurosci 26(29): 7555-7564.

67. Craig A (2003) A new view of pain as a homeostatic emotion. Trends Neurosci 26(6): 303-307.

68. Pittock SJ, Lucchinetti CF (2007) The pathology of MS: new insights and potential clinical applications. Neurologist 13(2): 45-56.

69. Mangiardi M, Crawford DK, Xia X, Du S, Simon FR, et al. (2011) An animal model of cortical and callosal pathology in multiple sclerosis. Brain Pathol 21(3): 263-278.

70. Iihara K, Joo DT, Henderson J, Sattler R, Taverna FA, et al. (2001) The influence of glutamate receptor 2 expression on excitotoxicity in Glur2 null mutant mice. J Neurosci 21(7): 2224-2239.